Energy & Environmental Science

ROYAL SOCIETY OF CHEMISTRY

PAPER

View Article Online
View Journal | View Issue

Cite this: *Energy Environ. Sci.*, 2021, **14**, 5491

High-performance PVDF membranes prepared by the combined crystallisation and diffusion (CCD) method using a dual-casting technique: a breakthrough for water treatment applications†

Vatsal Shah, [ab] Bo Wang[ab] and Kang Li *[ab]

Received 30th June 2021,
Accepted 23rd August 2021

DOI: 10.1039/d1ee02009a

rsc.li/ees

One of the most commonly used membranes for water treatment applications is polyvinylidene fluoride (PVDF) membranes prepared using the non-solvent induced phase separation (NIPS) method. Unfortunately, these membranes suffer from low permeances. The newly discovered combined crystallisation and diffusion (CCD) method, based on a unidirectional freezing approach, is a promising alternative to the NIPS method to make high-performance PVDF membranes. This work applies a novel but simple dual-casting technique to the CCD membranes, to substantially breach the limits of permeation performance set by the industry-favourite NIPS membranes without sacrificing the membranes' separation capabilities. Using this technique, one can tailor the specific properties of a CCD membranes' separation and support layers, by merely changing the dope compositions of the two cast layers. This is the first time that a technique such as this is so simple yet effective in producing pristine PVDF membranes with pure water permeances as high as 2400 LMH bar^{-1} and mean flow pore sizes as small as around 30 nm. The high permeances of these novel membranes will considerably improve the technological and economic feasibility of many ultrafiltration processes such as wastewater treatment and drinking water production.

Broader context

The scarcity of clean drinking water and effective wastewater treatment are some of the most challenging issues presented to the global community today. To deal with these, membrane filtration technology, particularly ultrafiltration, plays a vital role. The efficiency of a membrane is measured by its permeance, which is defined as the volume of liquid it can filter through a given membrane area under an applied pressure in a set time. Currently, most commercial PVDF membranes that are used for water-based ultrafiltration applications have pure water permeances around 50–200 LMH bar^{-1} with pore sizes in the range of 20–50 nm. For any filtration application, the higher the permeance of a membrane, the lower the total membrane area requirement will be. This will help reduce the capital cost and also the operating cost due to the reduced maintenance. The increase in permeance however, should not come at the expense of the membrane's separation performance, which many a time is the case. In this study, with the novel dual-casting approach that is applied to the newly discovered CCD method, PVDF membranes with pure water permeances as high as 2400 LMH bar^{-1} can be produced while still ensuring the membrane pore sizes remain unchanged (~30 nm) to maintain the separation efficiency. This suggests that this simple but effective approach is a promising alternative to the current industrial methods of production and shall help improve the overall adoptability of membrane-based filtration technologies.

Introduction

Given the enormous challenge of water scarcity that the world faces today, with many affluent cities around the globe like Cape Town and Chennai facing record droughts and imminent "Day Zeros", effective water management has become extremely important and the role of membrane filtration technology in dealing with the same shall be significant.[1–4] Of the many filtration processes, ultrafiltration (UF), which utilises membranes of pore size around 2–50 nm, is of particular importance as it is capable of filtering out most bacteria and viruses and renders water safe for drinking.[5–7] It is also important in the treatment of municipal and industrial wastewater to reduce the pollution being discharged out as effluent to the environment.[4,8] Even seawater desalination, another popular drinking water production route in many parts of the world,

[a] *Barrer Centre, Imperial College London, London SW7 2AZ, UK. E-mail: kang.li@imperial.ac.uk*
[b] *Department of Chemical Engineering, Imperial College London, London SW7 2AZ, UK*

† Electronic supplementary information (ESI) available. See DOI: 10.1039/d1ee02009a

involves ultrafiltration as a pretreatment step to reverse osmosis (RO).[9,10]

Among several materials used for making UF membranes, polyvinylidene fluoride (PVDF) is one of the most commonly used materials for water treatment applications as not only does it have excellent mechanical strength[11] and high thermal[12] and chemical resistance,[13] but it can also withstand chlorine disinfection.[14,15] The most commonly practised method for making PVDF UF membranes is the non-solvent induced phase separation method (NIPS). It is a well-established method, followed for decades now, where the membranes produced have an asymmetric morphology.[14,15] The tight-skin like separation layer, ensures efficient separation at the surface itself, which makes them highly desirable for UF applications. The NIPS method has many influencing parameters that need to be controlled effectively to maintain a consistent batch quality.[16] One of the main drawbacks however, of these NIPS-made PVDF UF membranes is that they suffer from low permeances and have a wide pore size distribution.[15,17–20]

Many researchers have tried various modification strategies to improve the permeances of PVDF UF membranes.[14,15] These include either using different solvents or solvent mixtures,[21–23] trying different additives,[23–28] or even changing the coagulation bath conditions.[29–31] These do increase the permeation performance of the membrane, but do so only marginally or at the cost of the membrane's separation capabilities. Table S1 in the ESI† presents the results of pore sizes and pure water permeances compiled from various such studies. As can be seen from Table S1 (ESI†), using graft copolymer in the dope solution can sometimes be very effective at improving the pure water permeances of PVDF-NIPS membranes.[32–35] But the mechanical strengths of the membrane deteriorate significantly because of the formation of the undesirably large macrovoids in its cross-section.[35–37] Its pore size distribution is also wide with pore sizes ranging from 20–160 nm.[32] This makes its application for commercial use rather challenging.

With regards to industry-standard PVDF UF membranes, most of them have pure water permeances around 50–200 litres per square meter membrane area per hour under 1 bar pressure difference across the membrane (see Table S2 in the ESI†).[20,38] To meet the operational needs of a filtration process, a larger membrane area is then required to compensate for this low permeance. This in turn limits the applicability of these PVDF filtration units in parts of the globe that are in dire need of effective and economical water treatment systems.

To address this challenge, a new membrane fabrication process called the Combined Crystallisation and Diffusion (CCD) method was developed by us.[20] It is a technique inspired by freeze-drying as it involves unidirectional cooling of the polymer cast solution using a solid media to freeze the solvent molecules into crystals. These crystals, after being leached out in an icy water bath, serve as pore templates in the final membrane.[20,38,39] To allow for the solvent crystal to grow, while the solvent molecules must diffuse towards the growing crystal, there must be counter diffusion of the polymer molecules away from the crystal and hence this process is called the combined crystallisation and diffusion method or CCD. This method employs DMSO as the solvent, as not only is it a greener and a more preferred alternative to other organic solvents,[40] but also has a relatively higher freezing point.[41]

The CCD membranes also have the preferred asymmetrical structure as a result of the rapid unidirectional cooling that is applied during the preparation. The low temperatures facilitate the crystallisation of solvent molecules, and the asymmetric membrane structure is determined by the temperature gradient developed in the cast layer.[39] The relatively colder end of the cast layer produces solvent crystals much smaller in size. Contrary to this, the warmer end has a much larger interconnected columnar crystal structure. Therefore, after the leaching of the solvent crystals, the result is an asymmetric porous membrane where the colder end forms a tight skin-like separation layer with high surface porosity, while the warmer end forms the support layer comprising interconnected microchannels. This unique structure is found to give the PVDF-CCD membranes significantly higher permeances and mechanical strengths than their NIPS counterparts without compromising the separation ability.[20] Moreover, the high permeance that is obtained using the CCD method is without the use of any pore-forming additives or additional processing requirements.

Other than the temperature gradient that largely decides the asymmetry, the concentration of the dope also affects the porous structure in the CCD membranes,[39] which offers us a powerful tool to further perfect the membrane structure. Based on the solvent crystal growth mechanism, we propose here that two different dope layers can be used as the support layer and the separation layer, respectively. The solvent crystal growth proceeds very differently in the two layers, which allows us to independently control one layer without affecting the other by varying the polymer dope concentrations. To implement such an approach, a dual-casting technique is applied where two layers of different polymer concentrations are cast. Here the top layer which forms the support uses a relatively lower polymer concentration to make the support layer more porous to substantially enhance the permeation properties while keeping the rejection properties unaffected.

Post fabrication, these dual-cast membranes are characterised for their mean flow pore sizes, pure water permeances (PWPs), and mechanical strengths, and are then compared to their single-cast counterparts.

Experimental

Membrane preparation

Single-cast membranes. Single-cast CCD membranes were prepared following a three-step process as illustrated in Fig. 1a. A single layer of polymer solution, with a thickness of 0.5 mm, was first cast on an aluminium casting plate (step 1). This plate was then placed on top of a precooled aluminium cooling plate at −30 °C (step 2) to cool and solidify the cast layer within a short period of time (< 3 s). After this, the solidified membrane

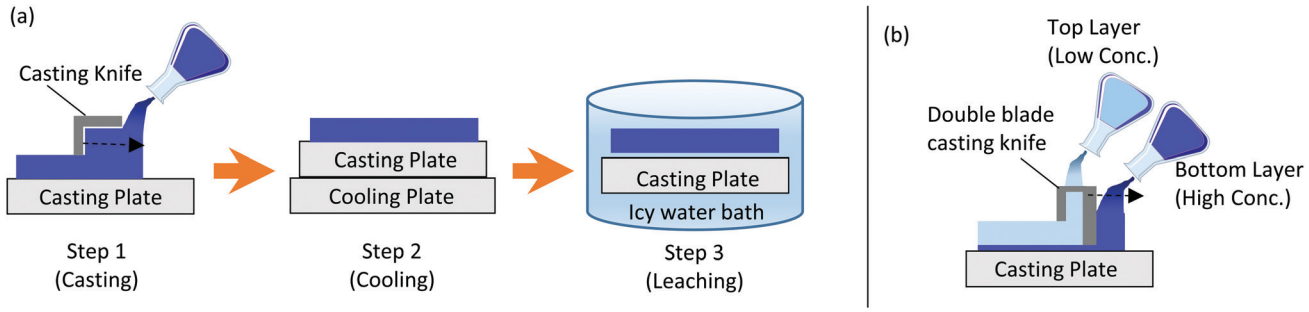

Fig. 1 Schematic showing (a) the three steps involved in CCD membrane fabrication; (b) the dual casting arrangement used.

was placed in an icy water bath to leach the solvent molecules out (step 3). The final membrane was then ready for filtration characterisation.

The preparation of single-cast NIPS membranes on the other hand was a two-step process where the prepared dopes were cast on a casting plate and then simply immersed in a water bath at room temperature to induce the phase separation.

PVDF-DMSO dope solutions with increasing polymer concentrations (10, 15 and 20 wt%) were investigated. The dope solutions were placed in an oven overnight at 80 °C to ensure complete dissolution of the polymer in the DMSO solvent. The dope solutions were then ready for casting and be made into membranes either *via* the NIPS or the CCD method. The membrane casting thickness was maintained at 0.5 mm for both CCD and NIPS membranes to allow for a fair comparison. Each batch of these single-cast membranes produced *via* either NIPS or CCD is given a sample ID. These are summarised in Table 1. A comparative study was then performed for both CCD and NIPS membranes made from these varying concentrations of PVDF dopes.

Dual-cast membranes. The preparation of dual-cast CCD membranes involved casting two layers of PVDF dope solutions at different concentrations, one on top of the other. The two layers were simultaneously cast using a specially designed, in-house built, two-blade casting knife. The bottom layer, which would determine the separation property, was cast using a high polymer concentration dope to produce a dense separation layer. The top layer, on the other hand, was cast using a lower polymer concentration dope to ensure that a higher porosity can be attained in the support. The casting thickness of the bottom layer was kept at 0.05 mm while that of the top layer was kept at 0.45 mm to keep the overall casting thickness of the dual-cast membrane at 0.5 mm, which is the same as what was kept for single-cast membranes. The schematic of the dual-cast arrangement is shown in Fig. 1b. The fabrication process then follows the same as that for single-cast CCD membranes (Fig. 1a). Two types of dual-cast CCD membranes were prepared where the bottom layer dope concentration was fixed at 20 wt%, while the top layer concentration varied. The sample ID allotted to the dual-cast CCD membranes along with the dope solution concentrations used for the casting of the two layers are summarised in Table 2.

Various materials used to make these membranes, along with the description of various characterisation techniques applied to the prepared membranes are detailed in the ESI.†

Results

Scanning electron microscopy

SEM images of the single-cast 20PVDF_CCD sample are presented in Fig. 2. They show the typical CCD membrane structure (Fig. 2a), where the membrane has a tight skin-like separation layer (Fig. 2d) and a porous support layer characterised by interconnected microchannels (Fig. 2e).[20,39] Comparatively, typical PVDF NIPS membranes have a tight skin in the separation layer along with large finger-like voids extending in the sponge-like support layer.[16,20,22,23,42] The SEM images of the cross-section and separation layer of the 20PVDF_NIPS membrane are presented in Fig. S1 in the ESI.†

The distinguishing features that contribute to higher permeances in CCD membranes are the high surface pore density and the interconnected and oriented microchannel structure that considerably reduces the membrane tortuosity (see section

Table 1 Sample IDs of the single-cast membranes with their corresponding dope concentration and preparation method

Sample ID[a]	PVDF dope conc. (wt%)	Preparation method
10PVDF_NIPS	10	NIPS
15PVDF_NIPS	15	NIPS
20PVDF_NIPS	20	NIPS
10PVDF_CCD	10	CCD
15PVDF_CCD	15	CCD
20PVDF_CCD	20	CCD

[a] Sample = "X"PVDF_"Y"."X" = PVDF dope conc. (wt%) used."Y" = preparation method.

Table 2 Sample IDs of the dual-cast CCD membranes with their corresponding dope concentrations used for casting the two layers

Sample ID[a]	Bottom layer PVDF dope conc. (wt%)	Top layer PVDF dope conc. (wt%)
20PVDF_10PVDF_CCD	20	10
20PVDF_15PVDF_CCD	20	15

[a] Sample = "X"PVDF_"Y"PVDF_CCD."X" = PVDF dope conc. (wt%) used to cast the bottom layer."Y" = PVDF dope conc. (wt%) used to cast the top layer.

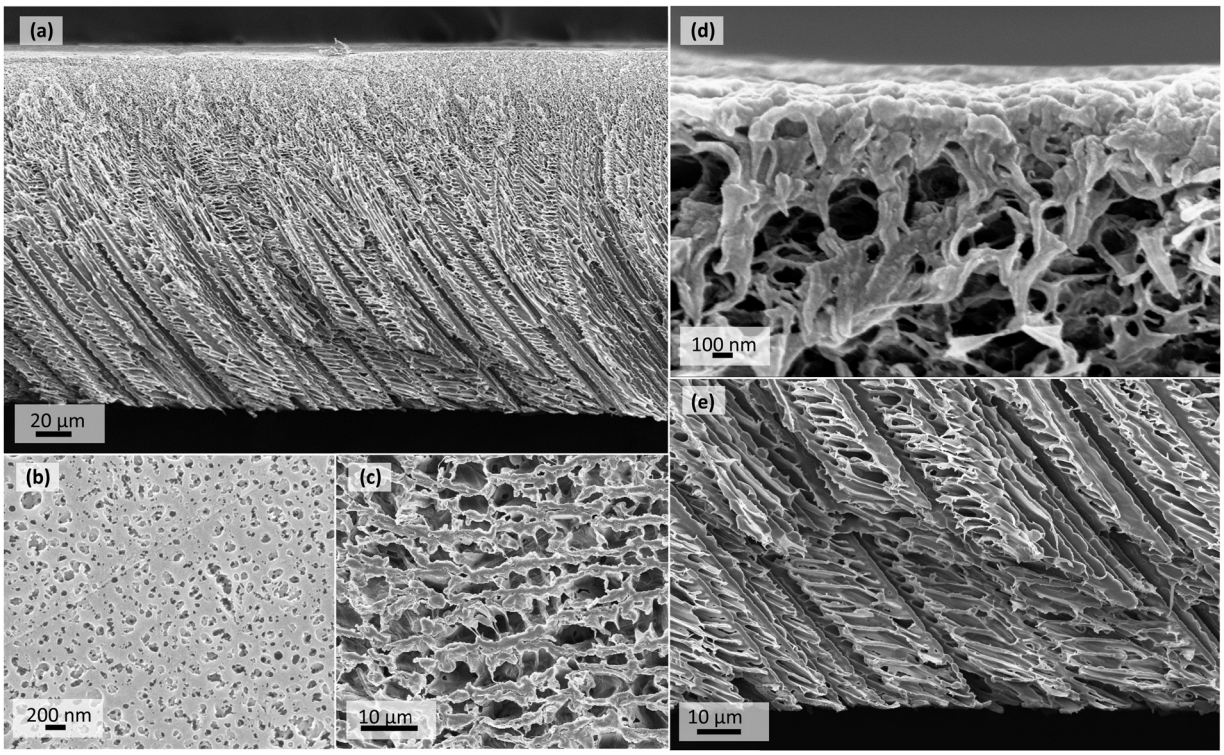

Fig. 2 SEM images of single-cast 20PVDF_CCD showing (a) the cross-sectional overview; (b) top surface view; (c) bottom surface view; (d) cross-sectional view of the separation layer; (e) cross-sectional view of the microchannels found in the support layer.

'Pure Water Permeance' below). NIPS membranes on the other hand have a low separation surface pore density and a large dead pore volume in the support layer.[20]

For dual-cast CCD membranes, SEM images of only the 20PVDF_10PVDF_CCD sample (Fig. 3) are presented here. This is because, given the higher concentration difference in the two cast layers of this membrane, the structural differences with the single-cast 20PVDF_CCD sample shall be more observable. The SEM images of 20PVDF_15PVDF_CCD are presented in Fig. S2 in the ESI.†

The top and bottom layers of the dual casting arrangement shown in Fig. 1b are seen in a reversed order in the SEM image cross-section of the dual-cast 20PVDF_10PVDF_CCD membrane (Fig. 3a). The thinner bottom cast layer of Fig. 1b represents the top separation layer in Fig. 3a, while the thicker top cast layer of Fig. 1b represents the bottom support layer in Fig. 3a. These two layers are represented using coloured arrows in Fig. 3a.

The cross-sectional view of the separation layer for the dual-cast membrane (Fig. 3d) looks just as tight as that of the single-cast one (Fig. 2d). In fact, the top view images of the separation surfaces (Fig. 2b and 3b) are almost identical. This is because for both the membranes, the region next to the casting plate had the same polymeric dope concentration at 20 wt%. The difference in the structure of the two membranes then depends on their support layers owing to the difference in the polymer concentration used to constitute that layer. While the single-cast membrane cross-section was composed of 20 wt% dope solution entirely including its support layer, the dual-cast membrane had its support layer composed of 10 wt% polymer dope. As a result, the size of the microchannels (Fig. 2e and 3e) and that of the pores as seen on the bottom view images (Fig. 2c and 3c) are much larger for the dual-cast membrane than they are for the single-cast membrane. This suggests that the size of the solvent crystals growing in the support layer would be larger for the former than it would be for the latter.

Fig. 4a–c present the SEM images of the cross-sectional, top and bottom views of the single-cast 10PVDF_CCD sample. The top view surface image of 10PVDF_CCD (Fig. 4b) does indeed have much larger pore sizes than both 20PVDF_CCD (Fig. 2b) and 20PVDF_15PVDF_CCD (Fig. 3b). The bottom view surface image (Fig. 4c), however, seems to have pores that are very similar in size to that of the dual-cast 20PVDF_10PVDF_CCD (Fig. 3c). Thus, it can be concluded that for the dual-cast membranes (in this case 20PVDF_10PVDF_CCD), the top separation side is very similar to that of a single-cast membrane prepared using a higher polymer concentration dope (in this case 20PVDF_CCD), while the bottom support side is very similar to that of a single-cast membrane prepared using a lower polymer concentration dope (in this case 10PVDF_CCD).

Dual-layered membranes have also been prepared in the past using traditional membrane manufacturing methods.[43,44] They usually use different polymer solutions to cast the two layers to tailor the membrane properties in a certain way. Many times, the two polymers may not be compatible with each other, which can result in instability and delamination between

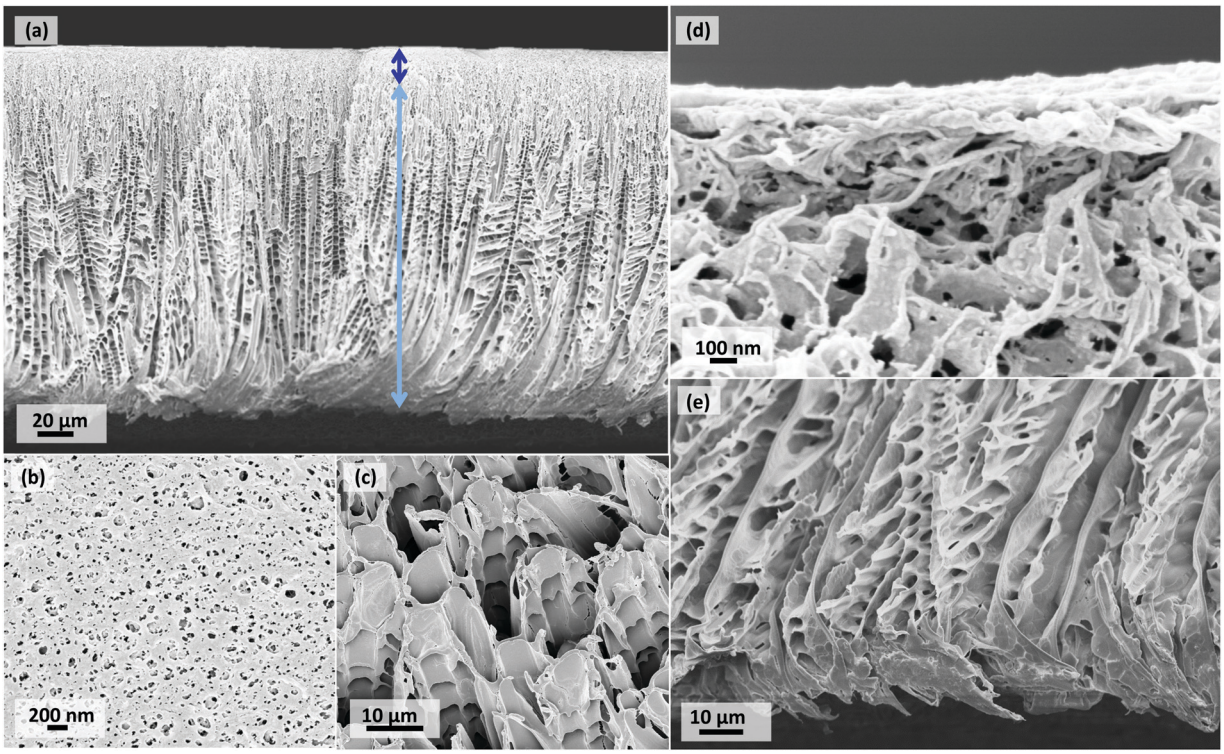

Fig. 3 SEM images of dual-cast 20PVDF_10PVDF_CCD showing (a) the cross-sectional overview; (b) top surface view; (c) bottom surface view; (d) cross-sectional view of the separation layer; (e) cross-sectional view of the microchannels found in the support layer.

the layers. However, the dual-casting technique used in this study uses the same polymeric solution but merely at different concentrations. As a result the dual-cast CCD membrane still appears as uniform as a single-cast one, with no distinct irregularities observed. This in turn eliminates any possibilities for delamination.

Mean flow pore size

Table 3 summarises the mean flow pore sizes for the various membranes that were prepared. For the single-cast membranes, as one would expect, an increase in the polymer dope concentration results in a decrease in the mean flow pore size. In fact, for the same polymer concentration dopes, both CCD and NIPS membranes have very similar pore sizes within experimental uncertainties, which implies that both should have similar rejection properties. For the dual-cast CCD membranes, the mean flow pore sizes are very similar to that of single-cast membranes prepared using 20 wt% PVDF dope, which means that the rejection properties of the two are very similar.

Fig. 4d then presents the pore size distribution of single-cast CCD membranes with their dual-cast counterpart. As can be seen the pore size distributions for all three CCD samples are rather narrow. This is in contrast to most NIPS membranes that have much wider pore size distributions.[14] From Fig. 4d, it can clearly be seen that the pore size distribution of dual-cast 20PVDF_15PVDF_CCD is identically similar to that of single-cast 20PVDF_CCD. The distribution of single-cast 15PVDF_CCD on the other hand is more so towards larger pore sizes. Similarly, Fig. S3 in the ESI† shows that the pore size distribution of 20PVDF_10PVDF_CCD also very much resembles that of 20PVDF_CCD, while 10PVDF_CCD have much larger pore sizes. This reinforces the fact that the concentration of the dope solution used in the region close to the casing plate can dictate the formation of the separation layer. Thus, one can tailor the rejection properties of the membrane by merely changing the concentration of the dope solution used for casting the bottom layer. Additionally, the concentration of the dope solution used for casting the top layer has little influence on the separation properties of the membrane.

Pure water permeance (PWP)

The PWP results for the single-cast membranes, presented in Fig. 4e, show that a decrease in the polymer dope concentration increases the PWP of the membrane. This is expected because a lower polymer concentration gives a membrane higher porosity and enlarged pores, which result in a reduced resistance to the water permeation flows. On comparing the permeation performance of CCD membranes to their NIPS counterparts, the former wins significantly over the latter in all three scenarios. The difference in permeation performance is substantial given that both the membrane types have similar mean flow pore sizes when prepared using the same polymer dope concentration.

Fig. 4f shows the PWP results of the dual-cast CCD membranes alongside the single-cast CCD and NIPS membranes prepared using 20 wt% polymer dope. All four samples,

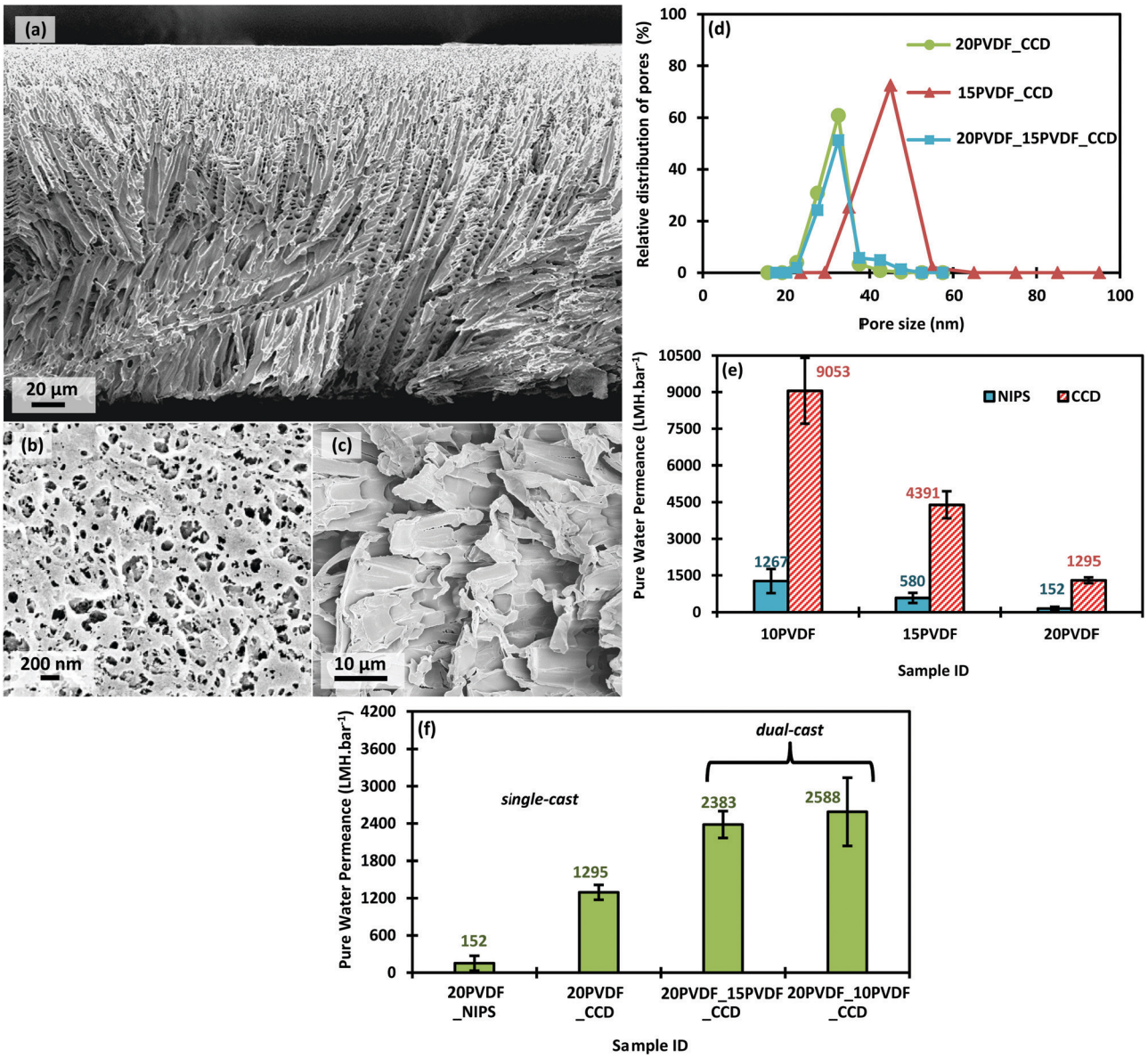

Fig. 4 Showing (a) cross-sectional overview, (b) top surface view and (c) bottom surface view of single-cast 10PVDF_CCD; (d) pore size distribution of 20PVDF_CCD, 15PVDF_CCD and 20PVDF_15PVDF_CCD; (e) pure water permeance comparison of single-cast CCD and NIPS membranes; (f) pure water permeance comparison of dual-cast CCD membranes with their single-cast counterparts that have similar pore sizes.

i.e. 20PVDF_NIPS, 20PVDF_CCD, 20PVDF_15PVDF_CDD and 20PVDF_10PVDF_CCD, that have almost the same mean flow pore sizes, have a significantly higher PWP for the latter two membranes that are produced *via* the dual-cast CCD route. While the tightness of the separation layer can be gauged by the mean flow pore size, the role of the support layer in contributing to the overall membrane transport resistance can be judged by the PWP measurement. The PWP of both the dual-cast CCD membranes is higher by almost 85% when compared to the single-cast CCD counterpart. This shows that in the dual-casting arrangement (Fig. 1b), the lower concentration dope that is used to cast the top thicker layer increases the porosity in the support, which in turn minimizes the overall flow resistance. The improvement in PWP in dual-cast CCD membranes is so high that on comparing them to the 20PVDF_NIPS membrane, the former have permeances that are higher than the latter by almost 15 times. This shows the potential of the dual-casting technique when applied to the CCD method, to obtain superior permeation performance, without compromising the membrane's rejection capabilities. On decreasing the concentration of the support layer in the dual-cast membrane from 15 wt% to 10 wt%, there is only a slight improvement in the PWP. This indicates that the resistance contribution of the separation layer, which is very similar in both the dual-cast membranes owing to the same dope concentration (20 wt%) used to cast this layer, now becomes the limiting factor.

It is for the first time that such high PWPs (2300–2600 LMH bar^{-1}) have been achieved for pure PVDF membranes in the ultrafiltration

Table 3 Mean flow pore sizes of single and dual-cast membranes

	Mean flow pore size (nm)	
Sample	CCD	NIPS
Single-cast membranes		
10PVDF	47 ± 4	45 ± 2
15PVDF	40 ± 3	36 ± 4
20PVDF	33 ± 2	33 ± 2
Dual-cast membranes		
20PVDF_10PVDF	27 ± 6	N/A
20PVDF_15PVDF	32 ± 1	N/A

range with pore sizes around 30 nm. Table S1 in the ESI† presents PWPs of UF PVDF membranes produced by other researchers using the NIPS process. Table S1 (ESI†) shows the PWP for pure PVDF membranes to be around 150 LMH bar^{-1}, similar to our in-house PVDF-NIPS membranes. The same is true for industry-standard commercial PVDF membranes (Table S2 in the ESI†).

Mechanical strengths

The tensile strengths of both single and dual-cast CCD membranes were investigated to gauge the differences in their mechanical properties. The result is presented in Table 4. It can clearly be seen that for the single-cast membranes as the polymer dope concentration decreases, the maximum load withstanding capacity and the tensile stress also decreases. Both the elongation and Young's modulus (= stress/strain), which indicates the resistance of the membranes to undergo deformation under stress, are significantly higher for 20PVDF_CCD compared to its lower concentration counterparts. This would be expected because, given the same membrane thickness, the membranes prepared with a lower polymer concentration have a lower mass per unit area, and hence a reduced capacity to withhold the load. As a result, the mechanical properties of the membrane deteriorate with a reduction in the polymer concentration.

The dual-cast CCD membranes have mechanical properties similar to those of the single-cast 10PVDF_CCD and 15PVDF_CCD samples, respectively. This is because the majority (90%) of the membrane composition of a dual-cast membrane is composed of the lower polymer dope concentration. Thus, although the PWP of 20PVDF_10PVDF_CCD was marginally higher than that of 20PVDF_15PVDF_CCD, there is a significant deterioration in the mechanical properties of the former compared to the latter. Hence, 20PVDF_15PVDF_CCD would be a better choice overall compared to its other dual-cast counterpart.

The PWP of 20PVDF_15PVDF_CCD was also tested for a longer duration of three hours and no reduction in permeance as a result of membrane compression was observed. This is due to the characteristic CCD membrane cross-section morphology. CCD membranes have oriented microchannels that increase in size from the separation layer to the support side and have PVDF grains that are tightly connected in between their walls.[20] Moreover, PVDF-CCD membranes are composed predominantly of β-phase and γ-phase PVDF crystals that give CCD membranes the high rigidity to high compression pressures.[20]

PVDF-NIPS membranes on the other hand have large finger-like voids and are composed mainly of the α-phase PVDF.[20] Our previous publication, which compared the mechanical properties of PVDF-CCD membranes with those of PVDF-NIPS membranes, showed that the former had much better resistance to high compression pressures than the latter.[20] The membranes were subjected to high pressure of 34.5 bar, where the CCD membrane retained its original morphology along with the overall membrane thickness while the NIPS membrane was severely compressed with a reduction in membrane thickness by almost 25%.

Discussion

The enhanced permeation performance of single-cast PVDF-CCD membranes relative to their NIPS counterparts can be attributed to the characteristic asymmetric structure of CCD membranes as seen in the SEM images in Fig. 2. During the CCD fabrication process, when the casting plate is placed in contact with the cooling plate, rapid heat dissipation occurs from one end of the casting plate. The polymer cast layer itself, however, is a poor conductor of heat, which results in a temperature gradient being established in the cast layer. The low temperatures facilitate the crystallisation of solvent molecules throughout the cast layer, but the extent of crystal growth, as described by Wang *et al.*,[39] is dependent on the temperature and polymer concentration gradients that are developed.

The growth of crystals can be described in three phases as illustrated in Fig. 5. In phase 1, solvent molecules nucleate heterogeneously from the metal plate surface and form a polymer-free solvent frozen front covering the surface of the plate. As a result, the polymer molecules are ejected out and form a thin layer of high polymer concentration locally next to this frozen front, resulting in a concentration gradient being established.

Phase 2 of crystal growth is in the thin region next to the frozen front, where the temperatures are still low. Here

Table 4 Tensile test results of both single and dual-cast CCD membranes

Sample	Thickness (mm)	Tensile stress (MPa)	Maximum load (N)	Elongation at maximum load (%)	Young's modulus (MPa)
10PVDF_CCD	0.19 ± 0.01	0.9 ± 0.1	2.0 ± 0.3	29 ± 04	24 ± 03
15PVDF_CCD	0.20 ± 0.02	1.6 ± 0.1	3.2 ± 0.4	36 ± 04	49 ± 7
20PVDF_CCD	**0.19 ± 0.01**	**2.7 ± 0.2**	**4.8 ± 0.5**	**41 ± 16**	**107 ± 16**
20PVDF_10PVDF_CCD	0.23 ± 0.02	1.1 ± 0.1	2.5 ± 0.3	33 ± 10	31 ± 03
20PVDF_15PVDF_CCD	**0.20 ± 0.01**	**1.7 ± 0.2**	**3.4 ± 0.6**	**44 ± 12**	**51 ± 05**

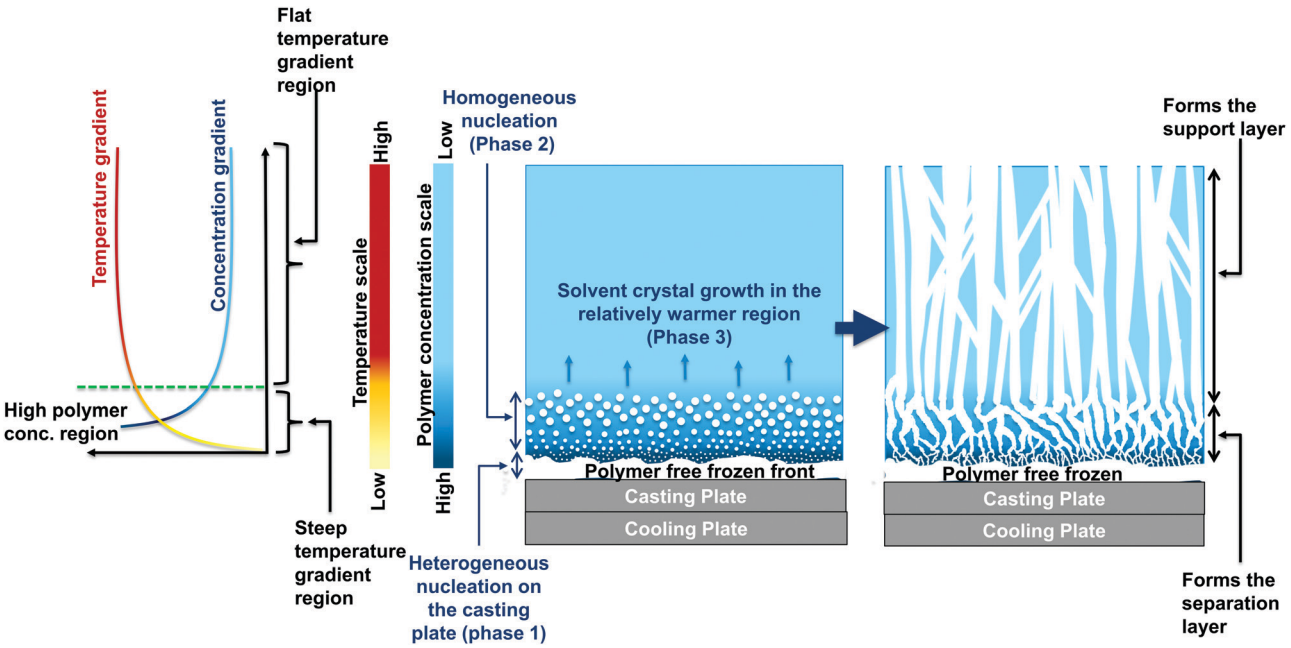

Fig. 5 Illustration of the crystal growth mechanism involved in CCD.

homogeneous nucleation of solvent molecules takes place and the size of these solvent crystals increases moving away from the frozen front, owing to both thermodynamic and kinetic factors. From a thermodynamic standpoint, a lower temperature and a higher polymer concentration favours phase separation through gelation, which limits the time for crystal growth. From the kinetic standpoint too, a high polymer concentration and low temperature result in a retardation of the polymer–solvent diffusion rates, which limits their exchange at the solvent crystal interface. Thus, in regions close to the casting plate where the polymer concentration is the highest and temperature the lowest, the size of solvent crystals homogeneously nucleated is the smallest. These solvent nuclei developed in phase 2 eventually grow and end up connecting each other, given the high volume fraction of the solvent that is present.

In the warmer end spectrum of the cast film, there isn't sufficient activation energy to allow for homogenous nucleation of the solvent crystals. Therefore, the solvent crystals that are homogenously nucleated in phase 2, continue to grow in this region in an oriented manner to form an interconnected cellular structure (phase 3).

After the leaching of the solvent crystals, the result is an asymmetric membrane, having a tight skin-like separation layer (the relatively cooler region of the cast layer-1st and 2nd phase) and a support layer that is characterised by a porous interconnected microchannel structure (the relatively warmer region-3rd phase). It is this structure that is responsible for high permeation performance in CCD membranes while keeping the rejections still intact.

The dual-casting technique tries to exploit the characteristic asymmetric structure of CCD membranes even further by using a relatively lower polymer concentration dope to cast the top thicker layer which eventually influences the support layer. The aim was to make this support layer more porous and have a lower transport resistance. The lower polymer concentration results in both a longer time for the solution surrounding the crystal to undergo gelation as well as enhances the polymer-solvent diffusion rates at the interface. This, therefore, results in the formation of larger diametrical cellular structures. This is particularly evident when one compares the cross-section and support side surface SEM images of the dual-cast 20PVDF_10PVDF_CCD membrane (Fig. 3c and e) to that of single-cast 20PVDF_CCD membrane (Fig. 2c and e). The former has a more porous support layer and larger support side pore sizes than the latter. Even the PWP results which show a significant enhancement in the permeation performance of dual-cast CCD membranes suggest that the porosity has indeed increased.

The bottom thinner layer, one in contact with the casting plate, which influences the separation property, is also polymer concentration-dependent. Using the same polymer dope concentration in the region next to the casting plate for both dual-cast and single-cast CCD membrane results in practically the same solvent-crystal structure in this region for both the membrane types. Both the mean flow pore sizes (Table 3) and the top view images of the separation surface (Fig. 2b and 3b) are therefore identical, which suggests them both having very similar rejection properties.

This, therefore, illustrates the possibility of influencing either the support or separation layer individually, by merely changing the dope composition of that layer.

The tensile stress test results give an insight into the practical implications that need to be considered when

applying the dual-casting technique. It suggests that decreasing the concentration of the top layer, which constitutes almost 90% of the membrane casting thickness, may have implications on the mechanical robustness of the membranes. This was evident in the case of 20PVDF_10PVDF_CCD and 20PVDF_15PVDF dual-cast CCD membranes, where although there was a marginal improvement in the permeance of the former compared to the latter, the mechanical properties were severely compromised in the former. Therefore, whenever the dual-casting technique is applied, an optimum concentration should be used to cast the top layer such that the enhancement in permeation properties is not at a significant cost in terms of the mechanical robustness of the membranes. An alternative to increasing the permeance even further but not compromising the mechanical properties of the membrane substantially would be to try and decrease the thickness of the separation layer while increasing the thickness of the support layer. This can be something for further investigation to see the effect of changing the casting layers' thicknesses while keeping the polymer dopes constituting these layers unchanged.

Conclusions

In this study, a new dual-casting approach was applied to the newly discovered CCD method to produce a first of its kind high-performance UF flat sheet PVDF membranes. The results showed that the dual-cast CCD membranes have pure water permeances higher by almost 15 times over the traditional NIPS counterpart, while still maintaining the separation pore sizes. The increase in permeance was not at the expense of the membrane's separation capabilities, but more as a consequence of high surface pore coverage and reduced transport resistance from the membrane's sub-layer, as was seen in the SEM images. It reaffirmed our hypothesis of the crystal growth mechanism involved in the CCD technique, which enables us to apply this casting approach and influence one of the layers of the membrane individually without affecting the other. The dual-casting technique is simple yet extremely effective with CCD membranes and allows one to breach the saturation limits reached in membrane performance very substantially. This significant breakthrough in permeation performance will consequently reduce the total membrane area required for any given filtration process and significantly bring down the capital and operating expenses. This would lead to an improvement in the economic viability of membrane-based water treatment systems and therefore result in its wider acceptance and application in several parts of the globe.

Author contributions

Vatsal Shah: conceptualization, methodology, software, validation, formal analysis, investigation, data curation, writing – original draft, writing – review and editing, visualization. Bo Wang: conceptualization, writing – review and editing. Kang Li: conceptualization, resources, writing – review and editing, supervision, project administration, funding acquisition.

Conflicts of interest

There are no conflicts to declare.

Acknowledgements

The authors gratefully acknowledge the research funding provided by EPSRC in the United Kingdom (Grant No. EP/R029180/1 and EP/R511547/1).

References

1 C. Y. Tang, Z. Yang, H. Guo, J. J. Wen, L. D. Nghiem and E. Cornelissen, *Environ. Sci. Technol.*, 2018, **52**, 10215–10223.
2 M. S. Ahmadi, J. Sušnik, W. Veerbeek and C. Zevenbergen, *Sustainable Cities Soc.*, 2020, **61**, 102295.
3 J. Brühl and M. Visser, *Water Resour. Econ.*, 2021, **34**, 100177.
4 A. Yusuf, A. Sodiq, A. Giwa, J. Eke, O. Pikuda, G. De Luca, J. L. Di Salvo and S. Chakraborty, *J. Cleaner Prod.*, 2020, **266**, 121867.
5 R. W. Baker, *Membrane Technology and Applications*, John Wiley & Sons, Ltd, Chichester, UK, 2012.
6 J. M. Arnal, B. Garcia-Fayos, G. Verdu and J. Lora, *Desalination*, 2009, **248**, 34–41.
7 E. Drioli, L. Giorno and E. Fontananova, *Comprehensive Membrane Science and Engineering*, Elsevier Science, 2017.
8 S. Al Aani, T. N. Mustafa and N. Hilal, *J. Water Proc. Eng.*, 2020, **35**, 101241.
9 R. Krüger, *Filtrat. Sep.*, 2009, **46**, 14–16.
10 J. Kavitha, M. Rajalakshmi, A. R. Phani and M. Padaki, *J. of Water Proc. Eng.*, 2019, **32**, 100926.
11 A. Pfenning, *Appl. Phys. Lett.*, 1995, **67**, 1022.
12 W. D. Benzinger, B. S. Parekh and J. L. Eichelberger, *Sep. Sci. Technol.*, 1980, **15**, 1193–1204.
13 J. Drobny, *Fluoroplastics*, Rapra Technology Limited, 2006.
14 G.-d. Kang and Y.-m. Cao, *J. Membr. Sci.*, 2014, **463**, 145–165.
15 F. Liu, N. A. Hashim, Y. Liu, M. R. M. Abed and K. Li, *J. Membr. Sci.*, 2011, **375**, 1–27.
16 J. T. Jung, J. F. Kim, H. H. Wang, E. di Nicolo, E. Drioli and Y. M. Lee, *J. Membr. Sci.*, 2016, **514**, 250–263.
17 G. R. Guillen, Y. Pan, M. Li and E. M. V. Hoek, *Ind. Eng. Chem. Res.*, 2011, **50**, 3798–3817.
18 M. Lee, B. Wang, Z. Wu and K. Li, *J. Membr. Sci.*, 2015, **483**, 1–14.
19 N. Hu, T. Xiao, X. Cai, L. Ding, Y. Fu and X. Yang, *Membranes*, 2016, **6**, 47.
20 B. Wang, J. Ji and K. Li, *Nat. Commun.*, 2016, **7**, 12804.
21 Q. Li, Z.-L. Xu and L.-Y. Yu, *J. Appl. Polym. Sci.*, 2010, **115**, 2277–2287.
22 A. Bottino, G. Camera-Roda, G. Capannelli and S. Munari, *J. Membr. Sci.*, 1991, **57**, 1–20.

23 M. L. Yeow, Y. T. Liu and K. Li, *J. Appl. Polym. Sci.*, 2004, **92**, 1782–1789.
24 E. Fontananova, J. C. Jansen, A. Cristiano, E. Curcio and E. Drioli, *Desalination*, 2006, **192**, 190–197.
25 H.-B. Li, W.-Y. Shi, Y.-F. Zhang, D.-Q. Liu and X.-F. Liu, *Polymers*, 2014, **6**.
26 N. Arahman, S. Mulyati, A. Fahrina, S. Muchtar, M. Yusuf, R. Takagi, H. Matsuyama, N. A. H. Nordin and M. R. Bilad, *Molecules*, 2019, **24**, 4099.
27 P.-Y. Zhang, H. Yang and Z.-L. Xu, *Ind. Eng. Chem. Res.*, 2012, **51**, 4388–4396.
28 E. Yuliwati and A. F. Ismail, *Desalination*, 2011, **273**, 226–234.
29 M. H. Razzaghi, M. Tavakolmoghadam, F. Rekabdar and F. Oveisi, *Water Environ. J.*, 2018, **32**, 366–376.
30 T. Wu, B. Zhou, T. Zhu, J. Shi, Z. Xu, C. Hu and J. Wang, *RSC Adv.*, 2015, **5**, 7880–7889.
31 D. Wang, K. Li and W. K. Teo, *J. Membr. Sci.*, 1999, **163**, 211–220.
32 B. Liu, C. Chen, T. Li, J. Crittenden and Y. Chen, *J. Membr. Sci.*, 2013, **445**, 66–75.
33 S. Wang, T. Li, C. Chen, B. Liu and J. C. Crittenden, *Front. Environ. Sci. Eng.*, 2017, **12**, 3.
34 Q. Wu, A. Tiraferri, H. Wu, W. Xie and B. Liu, *ACS Omega*, 2019, **4**, 19799–19807.
35 C. H. Loh and R. Wang, *Chin. J. Chem. Eng.*, 2012, **20**, 71–79.
36 M. M. Abed, S. Kumbharkar, A. Groth and K. Li, *Sep. Purif. Technol.*, 2013, **106**, 47–55.
37 S. Wang, T. Li, C. Chen, S. Chen, B. Liu and J. Crittenden, *Appl. Surf. Sci.*, 2018, **435**, 1072–1079.
38 V. Shah, B. Wang and K. Li, *J. Membr. Sci.*, 2021, **618**, 118708.
39 B. Wang, J. Ji, C. Chen and K. Li, *J. Membr. Sci.*, 2018, **548**, 136–148.
40 W. Xie, T. Li, C. Chen, H. Wu, S. Liang, H. Chang, B. Liu, E. Drioli, Q. Wang and J. C. Crittenden, *Ind. Eng. Chem. Res.*, 2019, **58**, 6413–6423.
41 W. S. MacGregor, *Ann. N. Y. Acad. Sci.*, 1967, **141**, 3–12.
42 S. P. Deshmukh and K. Li, *J. Membr. Sci.*, 1998, **150**, 75–85.
43 L. Setiawan, L. Shi, W. B. Krantz and R. Wang, *J. Membr. Sci.*, 2012, **423–424**, 73–84.
44 Q.-C. Xia, J. Wang, X. Wang, B.-Z. Chen, J.-L. Guo, T.-Z. Jia and S.-P. Sun, *J. Membr. Sci.*, 2017, **539**, 392–402.